


# Enhanced photoluminescence of monolayer $MoS_2$ on stepped gold structure

Yu-Chun Liu(刘玉春), Xin Tan(谭欣), Tian-Ci Shen(沈天赐), and Fu-Xing Gu(谷付星)
**Citation:**Chin. Phys. B, 2022, 31 (**8**): 087803. DOI: 10.1088/1674-1056/ac657b
Journal homepage: http://cpb.iphy.ac.cn; http://iopscience.iop.org/cpb

**What follows is a list of articles you may be interested in**

---

## Polarized photoluminescence spectroscopy in $WS_2$, $WSe_2$ atomic layers and heterostructures by cylindrical vector beams

Lijun Wu(吴莉君), Cuihuan Ge(葛翠环), Kai Braun, Mai He(贺迈), Siman Liu(刘思嫚), Qingjun Tong(童庆军), Xiao Wang(王笑), and Anlian Pan(潘安练)
Chin. Phys. B, 2021, 30 (**8**): 087802. DOI: 10.1088/1674-1056/abf3b6

## Faraday rotations, ellipticity, and circular dichroism in magneto-optical spectrum of moiré superlattices

J A Crosse and Pilkyung Moon
Chin. Phys. B, 2021, 30 (**7**): 077803. DOI: 10.1088/1674-1056/ac051f

## Thermally induced band hybridization in bilayer-bilayer $MoS_2/WS_2$ heterostructure

Yanchong Zhao(赵岩翀), Tao Bo(薄涛), Luojun Du(杜罗军), Jinpeng Tian(田金朋), Xiaomei Li(李晓梅), Kenji Watanabe, Takashi Taniguchi, Rong Yang(杨蓉), Dongxia Shi(时东霞), Sheng Meng(孟胜), Wei Yang(杨威), and Guangyu Zhang(张广宇)
Chin. Phys. B, 2021, 30 (**5**): 057801. DOI: 10.1088/1674-1056/abeee3

## Modulation of the second-harmonic generation in $MoS_2$ by graphene covering

Chunchun Wu(吴春春), Nianze Shang(尚念泽), Zixun Zhao(赵子荀), Zhihong Zhang(张智宏), Jing Liang(梁晶), Chang Liu(刘畅), Yonggang Zuo(左勇刚), Mingchao Ding(丁铭超), Jinhuan Wang(王金焕), Hao Hong(洪浩), Jie Xiong(熊杰), and Kaihui Liu(刘开辉)
Chin. Phys. B, 2021, 30 (**2**): 027803. DOI: 10.1088/1674-1056/abd77f

## Raman spectroscopy characterization of two-dimensional materials

Fang Liang(梁芳), Hejun Xu(徐何军), Xing Wu(吴幸), Chaolun Wang(王超伦), Chen Luo(骆晨), Jian Zhang(张健)
Chin. Phys. B, 2018, 27 (**3**): 037802. DOI: 10.1088/1674-1056/27/3/037802

---

# Enhanced photoluminescence of monolayer $MoS_2$ on stepped gold structure

Yu-Chun Liu(刘玉春), Xin Tan(谭欣), Tian-Ci Shen(沈天赐), and Fu-Xing Gu(谷付星)†

*School of Optical-Electrical and Computer Engineering, University of Shanghai for Science and Technology, Shanghai* 200093, *China*

(Received 9 February 2022; revised manuscript received 5 April 2022; accepted manuscript online 8 April 2022)

Different $MoS_2$/Au heterostructures can play an important role in tuning the photoluminescence (PL) and optoelectrical properties of monolayer $MoS_2$. Previous studies of PL of $MoS_2$/Au heterostructures were mainly limited to the PL enhancement by using different Au nanostructures and PL quenching of monolayer $MoS_2$ on flat Au surfaces. Here, we demonstrate the enhanced excitonic PL emissions of monolayer $MoS_2$/Au heterostructures on $Si/SiO_2$ substrates. By transferring the continuous monolayer $MoS_2$ onto a stepped Au structure consisting of 60-nm and 100-nm Au films, the $MoS_2$/Au-60 and $MoS_2$/Au-100 heterostructures exhibit enhanced PL emissions, each with a blue-shifted PL peak in comparison with the $MoS_2/SiO_2$. Furthermore, the PL intensity of $MoS_2$/Au-60 is about twice larger than that of $MoS_2$/Au-100. The different enhanced excitonic PL emissions in $MoS_2$/Au heterostructures can be attributed to the different charge transfer effects modified by the stepped Au structure. This work may provide an insight into the excitonic PL and charge transfer effect of $MoS_2$ on Au film and yield novel phenomena in $MoS_2$/Au heterostructures for further study of PL tuning and optoelectrical properties.

**Keywords:** $MoS_2$, stepped gold, heterostructures, enhanced photoluminescence

**PACS:** 78.67.–n, 78.55.–m, 71.35.–y, 71.35.Pq **DOI:** 10.1088/1674-1056/ac657b

## 1. Introduction

Molybdenum disulfide ($MoS_2$), as a typical two-dimensional (2D) transition metal dichalcogenides (TMDC), has drawn much attention due to its outstanding properties and various promising applications.[1–4] Numerous efforts have been made to tune excitonic photoluminescence (PL) and optoelectrical property of monolayer $MoS_2$, showing its great potentials in nanophotonics, micro-lasers, optoelectronic devices, *etc*.[5–8] These promising investigations indicate that the $MoS_2$/Au heterostructure plays an important role due to the surface plasmon resonance and charge transfer effects across the interface. Various Au nanostructures have been utilized to modulate the PL and optoelectrical performance of 2D $MoS_2$ through surface plasmon effect, including nanoparticles, nanorods, nanotriangles, nanoholes and nanostripe arrays.[9–14] The surface plasmons generated in the metallic nanostructures are conducive to generating excitons and achieving higher optical absorption via enhancing local-field coupling in $MoS_2$/Au heterostructures, leading to dramatic enhancement of PL and Raman emission.[15,16] Monolayer $MoS_2$ on Au grating array was used to explore the strong coupling regime of ultrafast plasmonic hot electron transfer, localized surface plasmons (LSPs) and surface plasmon polaritons (SPPs), where SPPs with a unique nonradiative feature can reuse the radiative energy of LSP and contribute to hot carrier generation.[17] Such prior researches suggest that the different $MoS_2$/Au heterostructures can create new phenomena and play an important role in tuning the PL and optoelectrical properties of monolayer $MoS_2$. However, these reported studies of $MoS_2$/Au heterostructures have mainly focused on different Au nanostructures.

Except for the surface plasmon effect due to Au nanostructures, the PL tailoring of monolayer $MoS_2$ by Au continuous thin films is still limited. The $MoS_2$/Au heterostructures can suppress the charge recombination by efficient charge transfer, which was critical for efficient exciton dissociation and good electron transport. The PL quenching of monolayer $MoS_2$ on flat Au surface by exfoliation method and by the chemical vapor deposition (CVD) method have been reported.[18,19] The PL quenching phenomenon observed in a $MoS_2$/Au junction was due to highly efficient interlayer charge transfer as compared with that in $MoS_2/SiO_2$.[20] The temperature increase and annealing processing reduced the interlayer spacings between the monolayer $MoS_2$ and metals, which can promote the interlayer charge transfer. It was also reported the vacuum annealing can induce the oxygen atoms to be removed from sulfur vacancies and reduce the inherent van der Waals gap at the $MoS_2$/Au interface, which facilitates the trapping of photo-generated electrons and the carrier separation.[21] Micro-Raman spectra revealed that the variation of out-of-plane $A_{1g}$ mode strongly is correlated with the strength of the $MoS_2$–Au interaction, which can be affected by the roughness and cleanliness of the underlying Au.[22] The Au substrates with $TiO_2$ spacer layers of different thickness values were reported to be able to enhance the PL emission of monolayer $MoS_2$ on Au due to the Fabry–Perot interference.[23,24] The

†Corresponding author. E-mail: gufuxing@usst.edu.cn

© 2022 Chinese Physical Society and IOP Publishing Ltd 

PL intensity of $MoS_2/TiO_2$/Au with a 41-nm-thick $TiO_2$ layer was observed to increase by 15 times, which is attributed to the fact that the local field enhancement originating from the metal surface roughness became dominant for thin spacer less than $\sim$ 10 nm. However, the evolution of excitonic PL change and electron transfer of the $MoS_2$/Au heterostructures have been still unclear so far. In the present work, we investigate the excitonic PL emission of continuous CVD-grown monolayer $MoS_2$ on Au thin film with a stepped structure. The enhanced PL emissions observed in the $MoS_2$/Au heterostructures in our experiments are different from the reported quenched or reduced PL emission from monolayer $MoS_2$ on the flat Au thin film. The A-excitonic PL emissions in $MoS_2$/Au-60 heterostructures exhibit 2.4-fold and 3.3-fold PL intensities at the peak energy, in comparison with those in $MoS_2$/Au-100 and $MoS_2/SiO_2$. The PL enhancement in $MoS_2$/Au heterostructure can be attributed to the different charge transfer effects.

## 2. Experimental method

The stepped Au structures with the thickness values of $\sim$ 60-nm and $\sim$ 100-nm Au were built by sputtering on an $Si/SiO_2$ substrate. $MoS_2$ monolayers were grown on $SiO_2$/Si substrates by the traditional CVD method in a furnace by using sulfur powder and molybdenum (VI) oxide powder as precursors.[25] Then the continuous $MoS_2$ monolayer was transferred to a target stepped Au structures on $SiO_2$/Si substrate by using poly(methyl methacrylate) (PMMA) and polydimethylsiloxanes (PDMS). After being transferred, the remaining $MoS_2$ on the target substrate was rinsed by acetone to remove organic residues. The 2D $MoS_2$/Au heterostructures were successfully built by transferring the $MoS_2$ monolayers onto the Au stepped structures with different thicknesses, respectively. The micro-PL and micro-Raman spectra were measured by a microscope system (Renishaw inVia) at room-temperature. The samples were excited by using a 532-nm (2.33 eV) continuous wavelength (CW) laser that is focused by a microscope objective lens ($\times$50) into an about 2-μm-diameter spot. The excitation power was kept less than 0.2 mW to minimize the laser heating effect. The surface morphology and surface potential of $MoS_2$ and Au films were measured using the atomic force microscopy (AFM, Bruker) under the atmospheric environment.

## 3. Results and discussion

The PL measurements of $MoS_2$/Au heterostructures consisting of monolayer CVD-grown $MoS_2$ and Au thin film were performed at room temperature under ambient atmosphere by using 532-nm CW-laser excitation. As shown in Fig. 1, the $MoS_2$/Au heterostructures exhibit enhanced PL emission with blue-shifted PL peak in comparison with $MoS_2/SiO_2$. The A-excitonic PL peaks are located at 1.871 eV, 1.891 eV, and 1.894 eV, respectively for $MoS_2$ monolayers transferred on $SiO_2$, Au (60 nm), and Au (100 nm). The PL peak of $MoS_2$ around 2.03 eV nm is attributed to the radiative recombination of B excitons. The excitonic PL emissions in $MoS_2$/Au-60 heterostructures exhibit 2.4-fold and 3.3-fold PL intensities in comparison with those of $MoS_2$/Au-100 and $MoS_2/SiO_2$.

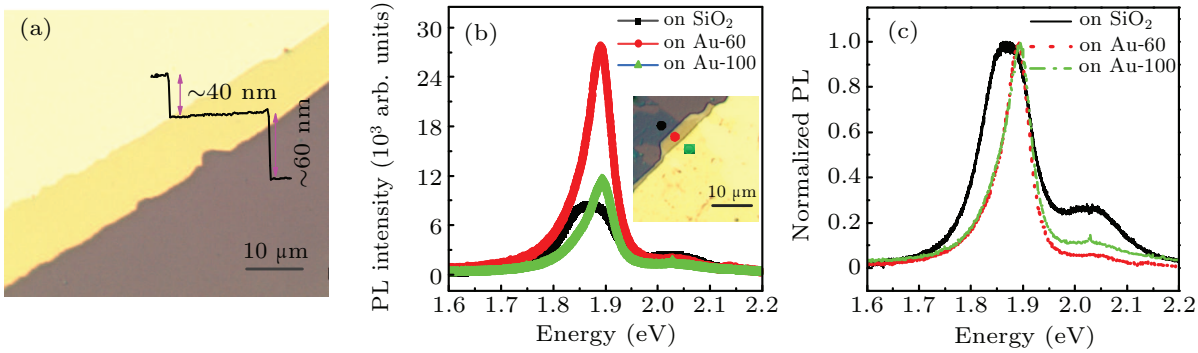



**Fig. 1.** (a) Optical image of $Si/SiO_2$ substrate and stepped Au structure with $\sim$ 60-nm and $\sim$ 100-nm-thick Au layer; (b) PL spectra and (c) normalized PL intensity for transferred continuous CVD-grown monolayer $MoS_2$ on $Si/SiO_2$, Au-60, and Au-100. Black, red, and green lines refer to the PL emissions of $MoS_2$ at the position of the black, red, and green dots in panel (b), respectively.

The PL spectra are fitted by Lorentzian curves with three peaks denoted by the emission of neutral excitons ($A_0$), trions ($A^-$), and B excitons at 1.895 eV, 1.855 eV, and 2.03 eV, respectively, as shown in Figs. 2(a)–2(c). Compared with $MoS_2$ on $SiO_2$, the $MoS_2$/Au (60 nm) heterostructure shows significant A-excitonic PL enhancement, and suppressed B excitonic PL, while the A-excitonic PL of $MoS_2$/Au (100 nm) decreases slightly. As shown in Figs. 2(d)–2(e), the excitonic PL intensity from $A_0$ ($I_{A_0}$) are obviously stronger than those form $A^-$ ($I_{A^-}$) in $MoS_2$/Au heterostructures. The estimated PL intensity ratio $A^-/A_0$ decreases from 4.03 in $MoS_2/SiO_2$ to 0.80 in $MoS_2$/Au-60, and 0.62 in $MoS_2$/Au-100. The $A^-$ recombination emission takes less spectral weight after the $MoS_2$ has been transferred onto the Au thin film than onto the $SiO_2$/Si, indicating the decrease of electron density in monolayer $MoS_2$/Au. The electron density $n_{el}$ in monolayer $MoS_2$ can be estimated from the trion PL spectral weight $I_{A^-}/I_{total}$ analysis according to mass action model based on the dy-

namic equilibrium among $A_0$, $A^-$, and free electrons as given below:[26]

$$n_{el} = \frac{I_{A^-}/I_{total}}{\frac{\gamma_{A^-}}{\gamma_{A_0}}\left(1-\frac{I_{A^-}}{I_{total}}\right)} \times \left[\left(\frac{4m_{A_0}m_e}{\pi\hbar^2 m_{A^-}}\right)k_B T \exp\left(-\frac{E_b}{k_B T}\right)\right], \quad (1)$$

where $k_B$ is the Boltzmann constant, $E_b$ is the trion binding energy ($\sim 20$ meV), $m_0$ is the mass of free electron, $m_e$ ($0.35m_0$), $m_{A_0}$ ($0.8m_0$), and $m_{A^-}$ ($1.15m_0$) are the effective mass of electron, $A_0$, and $A^-$, respectively, $\gamma_{A^-}/\gamma_{A_0}$ refers to the relative decay rate, and the value is $\sim 0.15$.[27]

As shown in Fig. 2(f), the corresponding estimated electron densities are $2.0\times10^{13}$ cm$^{-2}$ and $1.55\times10^{13}$ cm$^{-2}$ in $MoS_2$/Au-60 and $MoS_2$/Au-100 respectively, both of which are much smaller than that in $MoS_2/SiO_2$ ($1.01\times10^{14}$ cm$^{-2}$). The PL emissions from $MoS_2$ on Au are obviously higher than on $SiO_2$, which is also in agreement with a dominant PL contribution from $A_0$ emission in $MoS_2$/Au heterostructure with enhanced transition from $A^-$ to $A_0$. Furthermore, the B-excitonic PL emissions almost vanish in $MoS_2$/Au-60 and $MoS_2$/Au-100.

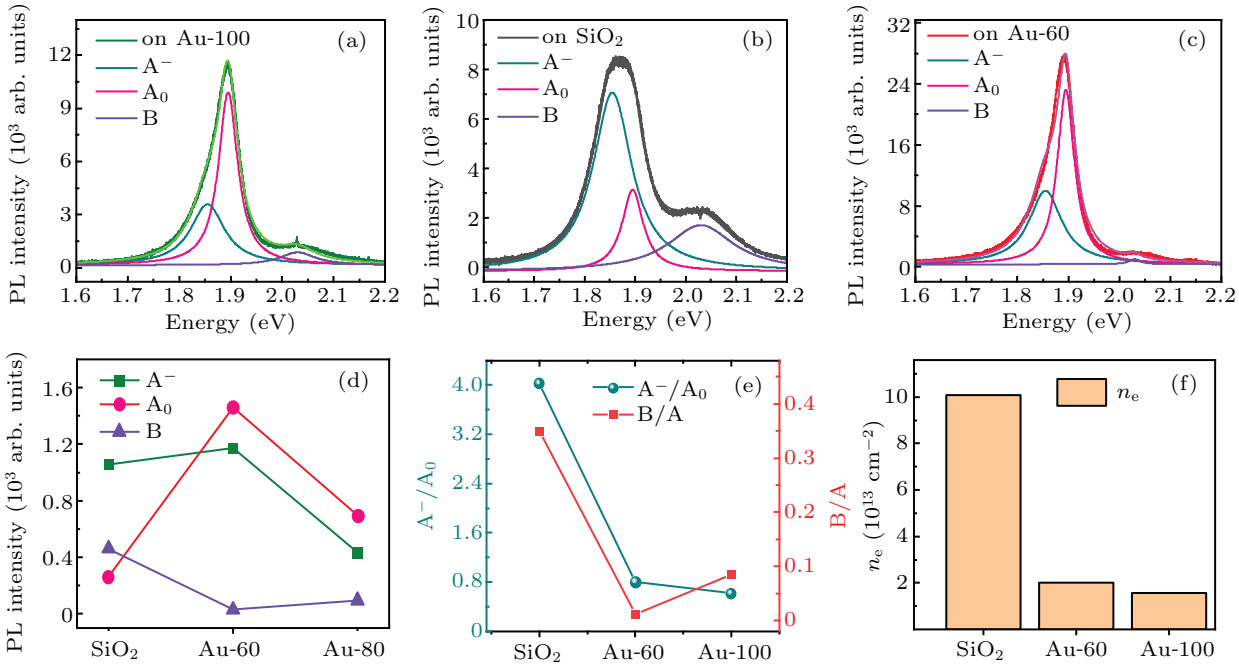



**Fig. 2.** (a)–(c) Representative PL spectra fitted by Lorenz function with three PL peaks ($A_0$, $A^-$, and B) for $MoS_2$ on $SiO_2$, Au-60, and Au-100; (d) PL intensity from $A_0$, $A^-$, and B, (e) PL spectral weights and (f) estimated electron density in $MoS_2$ on $SiO_2$, Au-60, and Au-100.

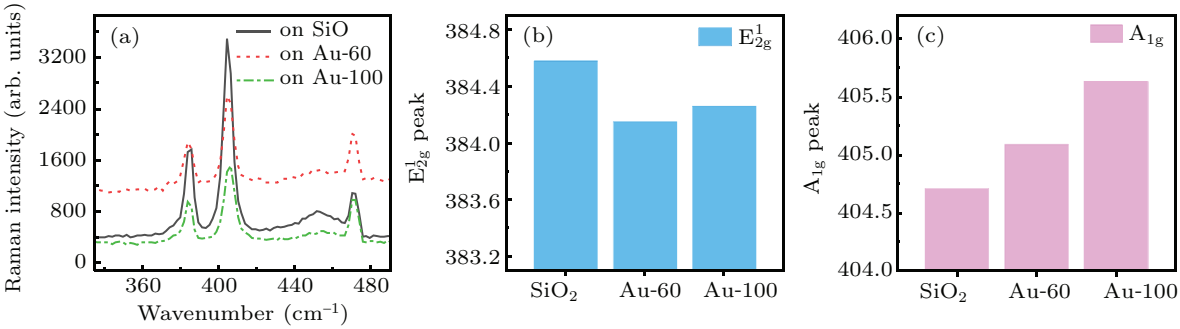



**Fig. 3.** (a) Raman spectra, (b) $E^1_{2g}$ peaks, and (c) $A_{1g}$ peaks for transferred $MoS_2$ on $SiO_2$, Au-60, and Au-100.

Generally, the enhanced PL intensity in $MoS_2$ can be ascribed to the chemical doping effect, the plasmon effect, the train effect, and charge transfer effect. There is no additional chemical doping in our experiment. Since the roughness of Au film is small ($< 1$ nm), the localized plasmon effect of $MoS_2$ on Au film is negligible in comparison with the effect of Au nanoparticles and Au plasmonic nanostructures. To uncover the enhanced PL emission in $MoS_2$/Au heterostructure, the transferred monolayer $MoS_2$ on $SiO_2$ and stepped Au are further characterized by Raman spectroscopy. Figure 3 shows that the Raman peaks of $MoS_2$ on $SiO_2$ are at 384.58 cm$^{-1}$, which is caused by the in-plane vibration of S–Mo–S atom ($E^1_{2g}$ mode), and 404.71 cm$^{-1}$, which is induced by the out-of-plane vibration of S atoms ($A_{1g}$ mode). The frequency difference in frequency between the Raman peaks of the transferred monolayer $MoS_2$ on the $SiO_2$/Si struc-

ture is 20.13 $cm^{-1}$, in accordance with the reported value of transferred monolayer $MoS_2$. The $E^1_{2g}$ and $A_{1g}$ peaks of Raman spectra are 384.15 $cm^{-1}$ and 405.09 $cm^{-1}$ for $MoS_2$/Au (60 nm), and 384.26 $cm^{-1}$ and 405.63 $cm^{-1}$ for $MoS_2$/Au (100 nm). The obvious red shift of $E^1_{2g}$ peak and the blue shift of the $A_{1g}$ peak for $MoS_2$/Au with respect to $MoS_2$ on $SiO_2$ are observed. The $A_{1g}$ peak is obviously shifted by $\sim 0.92$ $cm^{-1}$, indicating interaction between $MoS_2$ and Au. The difference in frequency between $E^1_{2g}$ and $A_{1g}$ peak positions of $MoS_2$ on Au-60 and Au-100 are $\Delta\omega_{Au-60} = 20.94$ $cm^{-1}$ and $\Delta\omega_{Au-100} = 21.37$ $cm^{-1}$, respectively.

Generally, $E^1_{2g}$ and $A_{1g}$ peak shifts are associated with the strain and doping effect in $MoS_2$. Raman peak shifts vary linearly with biaxial strain (from 0 to 1%), and the slopes are $-4.48$ $cm^{-1}$ and $-1.02$ $cm^{-1}$ per 1% of biaxial strain for $E^1_{2g}$ and $A_{1g}$ modes, respectively, while the A exciton peak exhibits a linear red-shift rate of $-0.11$ eV per 1% of biaxial tensile strain.[28] Furthermore, the electron doping density of $1.8 \times 10^{13}$ $cm^{-2}$ could lead to $-4$-$cm^{-1}$ shift in the $A_{1g}$ mode and $-0.6$-$cm^{-1}$ shift in the $E^1_{2g}$ mode.[29] It has been reported that $A_{1g}$ mode exhibits peak shift mostly dependent on the charge doping, while $E^1_{2g}$ mode was more sensitive to the tensile strain resulting from $MoS_2$.[30–32] Comparing with the reference case of a freestanding 1-L $MoS_2$ with $E^1_{2g}$ and $A_{1g}$ peak frequencies at 385 $cm^{-1}$ and 405 $cm^{-1}$, the biaxial tensile strain and n-type doping (electron-doping) for $MoS_2$ on $SiO_2$ are estimated at $\sim 0.087\%$ and $0.91 \times 10^{12}$ $cm^{-2}$, respectively. A strain and a p-type doping density in $MoS_2$/Au-60 are estimated at $\sim 0.200\%$ and $\sim 1.32 \times 10^{12}$ $cm^{-2}$, while the tensile strain and p-type doping (hole-doping) in $MoS_2$/Au-100 are estimated at $\sim 0.193\%$ and $\sim 3.72 \times 10^{12}$ $cm^{-2}$, respectively. The negligible difference in tensile strain suggests that there is no obvious difference in strain effect between $MoS_2$/Au-60 heterostructure and $MoS_2$/Au-100 heterostructure. The estimated p-type doping in $MoS_2$/Au can be attributed to the electron transferring from $MoS_2$ to Au, which is in agreement with excitonic PL emission result. Since the A-excitonic PL can exhibit a linear peak red-shifting and rapid intensity decreasing with biaxial tensile strain increasing,[33,34] the greater enhancement of PL intensity in $MoS_2$/Au-60 is due to the difference in electron transfer effect rather than the small strain effect difference between $MoS_2$/Au-60 and $MoS_2$/Au-100. Furthermore, the Raman intensity per area from the suspended region was reported to be 50%–100% higher than that from the supported region in the literature.[35] The higher intensity in $MoS_2$/Au-60 than in $MoS_2$/Au-100 can be attributed to the less contact between $MoS_2$ layer and Au-60, which is in accord with the above estimated p-type doping density.

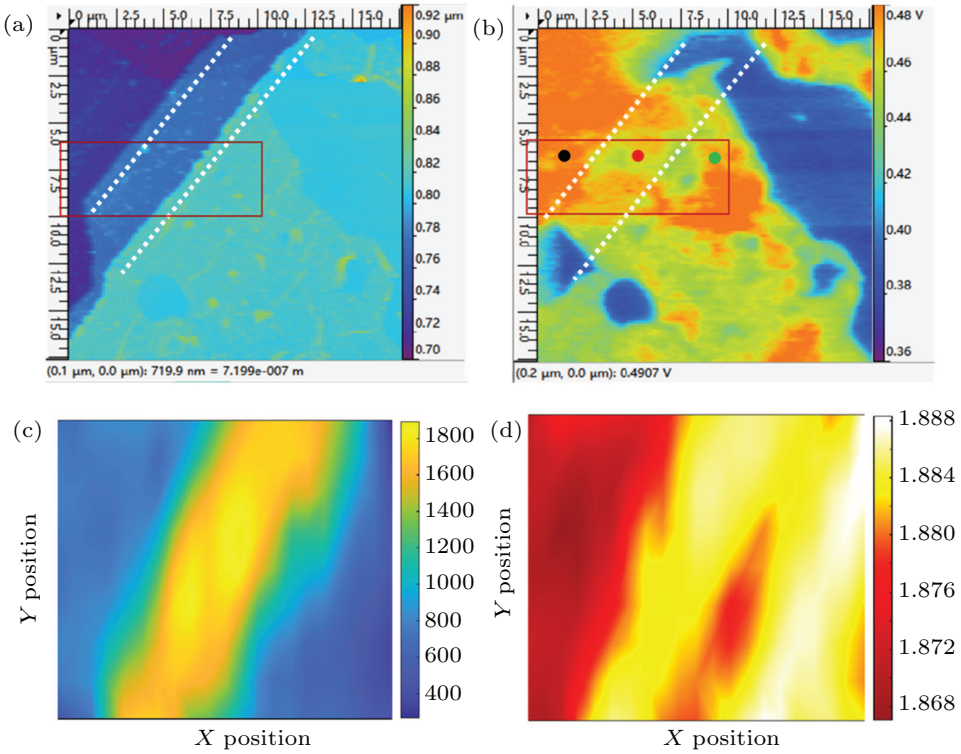



**Fig. 4.** (a) and (b) Morphology and SKPM surface potential, (c) PL intensity mapping, (d) PL emission peak mapping for monolayer $MoS_2$ transferred on $Si/SiO_2$ and stepped Au structure.

To further study the charge transfer between $MoS_2$ and underlying substrate, scanning Kelvin probe microscopy (SKPM) measurement with an ElectriMulti75-G probe is carried out so as to obtain the morphology and surface potential information of samples simultaneously. The surface potential of monolayer $MoS_2$ and Au can be measured by the contact potential difference, which refers to the difference in work function between tip ($\phi_{tip}$) and sample ($\phi_{tip}$), thus

$eV_{surf} = (\phi_{tip} - \phi_{sample})$. The morphology and surface potential of $MoS_2/SiO_2$and $MoS_2$/Au heterostructures are shown in Figs. 4(a) and 4(b). The difference in measured contact potential of $MoS_2/SiO_2$ (black dot), $MoS_2$/Au-60 (red dot), and $MoS_2$/Au-100 (green dot) are 0.490 V, 0.470 V, and 0.480 V, respectively, while the contact potential difference of Au is 0.383 V. In contrast with the work function of Au ($\sim$ 5.1 eV), surface work function of $MoS_2/SiO_2$, $MoS_2$/Au-60, and $MoS_2$/Au-100 without laser illumination are 4.993 eV, 5.013 eV, and 5.003 eV, respectively. According to the 2D model of electron gas at non-zero temperature, the Fermi energy shift in $MoS_2$ monolayer ($\Delta E_F = \pi\hbar^2\Delta n/m_e$) can be calculated from the electron density change by using an electron band mass of $m_e = 0.35m_0$, where $m_0$ is the electron mass. Comparing with $MoS_2$ on $SiO_2$, the surface potential of $MoS_2$/Au-60 and $MoS_2$/Au-100 are reduced by 20 mV and 10 mV, respectively, indicating that the calculated electron density differences are $2.92\times10^{12}$ cm$^{-2}$ and $1.46\times10^{12}$ cm$^{-2}$, respectively. The calculated electron density differences from surface potential without laser illumination are much smaller than that estimated from $A^-/A_0$ ratio, suggesting that the electron density of $MoS_2$ is increased under laser illumination.

Figures 4(c) and 4(d) refer to the PL intensity mapping and PL peak mapping of $MoS_2$ in the region of black rectangle in Fig. 4(a). The difference in PL intensity in $MoS_2/SiO_2$, $MoS_2$/Au-100, and $MoS_2$/Au-60 can be attributed to the different charge transfer situations. As Kwon *et al.* reported, the measured surface potential of monolayer $MoS_2$ in contact with the Au stripe in dark is greater than that of the suspended $MoS_2$ surface, while the surface potential of $MoS_2$ on Au stripe is smaller than that of the suspended $MoS_2$ surface under light illumination with a wavelength of 532 nm.[36] Furthermore, Li *et al.* reported that the work function is 4.93 eV for CVD-grown monolayer $MoS_2$ on an $Si/SiO_2$ substrate and 5.50 eV for that on a Pt substrate in dark, which decreases to 4.74 eV and increases to 5.56 eV under 355-nm laser excitation, respectively.[37] Therefore, we consider that the work function of $MoS_2/SiO_2$ will decrease, and the work function of $MoS_2$/Au-60 will be higher than that of $MoS_2$/Au-100 under 532-nm laser excitation. Thus, the excess electrons in $MoS_2$/Au-100 can move towards the $MoS_2$/Au-60 under laser illumination as shown in Fig. 5(a). Additionally, the electrons in $MoS_2$/Au-100 can also be readily transferred into the Au film at the $MoS_2$/Au interface. Thus, as shown in Fig. 5(b), the electrons transfer in $MoS_2$ occurs between $MoS_2/SiO_2$, $MoS_2$/Au and the underlying Au film, which will finally lead to a transient dynamic equilibrium and band alignment under the laser excitation.[38] As a result, the decreasing of electron density in $MoS_2$/Au gives rise to the blue-shift of PL peak and PL enhancement of $A_0$ radiative recombination. It should be noted that the laser used in our study has a size of $\sim$ 2 μm in diameter and average power of less than 0.2 mW. During the PL measurement, $MoS_2/SiO_2$, $MoS_2$/Au-100, and $MoS_2$/Au-60 cannot be irradiated simultaneously. The photo-induced electrons from irradiated $MoS_2$ region can drift to um-irradiated region. The dynamic equilibrium will be different when the laser irradiates the $MoS_2/SiO_2$, $MoS_2$/Au-100, and $MoS_2$/Au-60, respectively. In addition, since $O_2/H_2O$ molecules from ambient air can be physically and chemically adsorbed by the defects on $MoS_2$ surface, the charge transfer can also occur between monolayer $MoS_2$ and gas molecules. The PL emission of $MoS_2$/Au heterostructures can be tuned by changing the charge transfer between $MoS_2$ and gas molecules, which will be further investigated in the future.

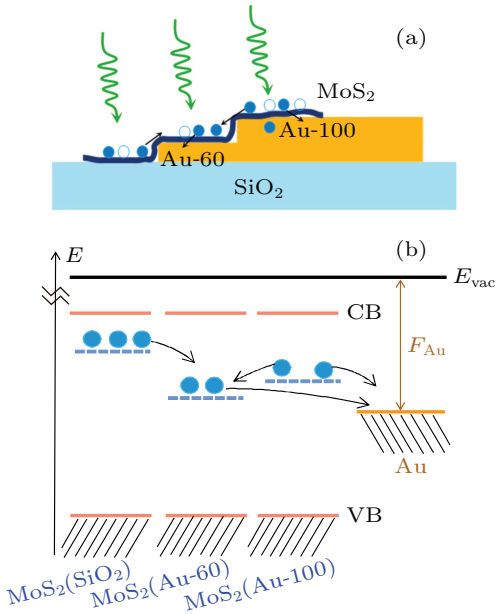



**Fig. 5.** Schematic illustrations of (a) charge transfer and (b) expected electron transfer at Fermi energy levels between $MoS_2/SiO_2$, $MoS_2$/Au, and underlying Au under laser excitation.

## 4. Conclusions and perspectives

In this work, we have built $MoS_2$/Au heterostructures by transferring CVD-grown monolayer $MoS_2$ onto a stepped Au structure with Au thickness of $\sim$ 60 nm and $\sim$ 100 nm on $Si/SiO_2$ substrate. The $MoS_2$/Au-60 and $MoS_2$/Au-100 heterostructures exhibit enhanced PL emission with blue-shifted PL peaks in comparison with $MoS_2/SiO_2$. Furthermore, the PL intensity of the $MoS_2$/Au-60 sample is twice larger than that of the $MoS_2$/Au-100 sample. The difference in enhancement extent of excitonic PL among the $MoS_2$/Au heterostructures can be attributed to the difference in their charge transfer effects modified by the stepped Au structure, which determines the PL emission from $A_0$ and $A^-$. Our results demonstrate a novel method to quantitatively tune the excitonic PL emission from $MoS_2$/Au vertical heterostructure, and are also conducive to the understanding of the charge transfer between

CVD-grown $MoS_2$ and Au, and provide a valuable insight into the excitonic PL and optoelectrical properties of $MoS_2$/metal heterostructures.

## Acknowledgements

We thank Dr. Zhaoqi Gu and Prof. Jiaxin Yu for helpful suggestions.

Project supported by the China Postdoctoral Science Foundation (Grant No. 2020M671168) and the National Natural Science Foundation of China (Grant No. 62075131).

## References

[1] Li N, Wang Q, Shen C, Wei Z, Yu H, Zhao J, Lu X, Wang G, He C, Xie L, Zhu J, Du L, Yang R, Shi D and Zhang G 2020 *Nat. Electron.* **3** 711
[2] Mouloua D, Kotbi A, Deokar G, Kaja K, Marssi M E, Khakani M A E and Jouiad M 2021 *Materials* **14** 3283
[3] Liu Y C and Gu F X 2021 *Nanoscale Adv.* **3** 2117
[4] Mouri S, Miyauchi Y and Matsuda K 2016 *Appl. Phys. Express* **9** 055202
[5] Su H, Wu S, Yang Y, Leng Q, Huang L, Fu J, Wang Q, Liu H and Zhou L 2021 *Nanophotonics* **10** 975
[6] Liao F, Yu J, Gu Z, Yang Z, Hasan T, Linghu S, Peng J, Fang W, Zhuang S, Gu M and Gu F 2019 *Sci. Adv.* **5** eaax7398
[7] Luo Y, Shan H, Gao X, Qi P, Li Y, Li B, Rong X, Shen B, Zhang H, Lin F, Tang Z and Fang Z 2020 *Nanoscale Horiz.* **5** 971
[8] Shen T, Li F, Zhang Z, Xu L and Qi J 2020 *ACS Appl. Mater. Interfaces* **12** 54927
[9] Cao S, Hou L, Wang Q, Li C, Yu W, Gan X, Liu K, Premaratne M, Xiao F and Zhao J 2021 *Photon. Res.* **9** 501
[10] Wang Z, Liu J, Fang X, Wang J, Yin Z, He H, Jiang S, Zhao M, Yin Z, Luo D, Shum P and Liu Y J 2021 *Nanophotonics* **10** 1733
[11] Yu L, Liu D, Qi X Z, Xiong X, Feng L T, Li M, Guo G P, Guo G C and Ren X F 2018 *Chin. Phys. B* **27** 047302
[12] Garai M, Zhu Z, Shi J, Li S and Xu Q H 2021 *J. Chem. Phys.* **155** 234201
[13] Kim E, Lee C, Song J, Kwon S, Kim B, Kim D H, Park T J, Jeong M S and Kim D W 2020 *J. Phys. Chem. Lett.* **11** 3039
[14] Yu L, Liu D, Qi X Z, Xiong X, Feng L T, Li M, Guo G P, Guo G C and Ren X F 2018 *Chin. Phys. B* **27** 047302
[15] Holmi J T, Raju R, Ylönen J, Subramaniyam N and Lipsanen H 2021 *Superlattice Microst.* **160** 107077
[16] Yang Y, Liu W G, Lin Z T, Pan R H, Gu C Z and Li J J 2021 *Mater. Today Phys.* **17** 100343
[17] Shan H, Yu Y, Wang X, Luo Y, Zu S, Du B, Han T, Li B, Li Y, Wu J, Lin F, Shi K, Tay B K, Liu Z, Zhu X and Fang Z 2019 *Light Sci. Appl.* **8** 9
[18] Bhanu U, Islam M. Tetard L and Khondaker S I 2014 *Sci. Rep.* **4** 5575
[19] Pollmann E, Sleziona S, Foller T, Hagemann U, Gorynski C, Petri O, Madauß L, Breuer L and Schleberger M 2021 *ACS Omega* **6** 15929
[20] Zhang L, Yan H, Sun X, Dong M, Yildirim T, Wang B, Wen B, Neupane G P, Sharma A, Zhu Y, Zhang J, Liang K, Liu B, Nguyen H T, Macdonald D and Lu Y 2019 *Nanoscale* **11** 418
[21] Shen T, Lu X, Xu L, Li Z and Qi J 2020 *Nanosci. Nanotech. Lett.* **12** 141
[22] Velický M, Rodriguez A, Bouša M, Krayev A V, ondráček M, Honolka J, Ahmadi M, Donnelly G E, Huang F, Abruña H D, Novoselov K S and Frank O 2020 *J. Phys. Chem. Lett.* **11** 6112
[23] Jeong H Y, Kim U J, Kim H, Han G H, Lee H, Kim M S, Jin Y, Ly T H, Lee S Y, Roh Y G, Joo W J, Hwang S W, Park Y and Lee Y H 2016 *ACS Nano* **10** 8192
[24] Chen X, Zang J, Yang X, Zhang Y, Chen Y, Zhao Y, Dong L and Shan C X 2022 *Sci. China-Mater.* **65** 1861
[25] Wang S, Xu Y and Liu Y 2020 *Acta Photon. Sin.* **49** 0316002
[26] Li Y, Qi Z, Liu M, Wang Y, Cheng X, Zhang G and Sheng L 2014 *Nanoscale* **6** 15248
[27] Mouri S, Miyauchi Y and Matsuda K 2013 *Nano Lett.* **13** 5944
[28] Li H, Contryman A W, Qian X F, Ardakani S M, Gong Y J, Wang X L, Weisse J M, Lee C H, Zhao J H, Ajayan P M, Li J, Manoharan H C and Zheng X L 2015 *Nat. Commun.* **6** 7381
[29] Chakraborty B, Bera A, Muthu D V S, Bhowmick S, Waghmare U V and Sood A K 2012 *Phys. Rev. B: Condens. Matter Mater. Phys.* **85** 161403
[30] Buscema M, Steele G A, Zant H S J and Castellanos-Gomez A 2014 *Nano Res.* **7** 561
[31] Ochedowski O, Marinov K, Scheuschner N, Poloczek A, Bussmann B K, Maultzsch J and Schleberger M 2014 *Beilstein J. Nanotechnol.* **5** 291
[32] Yang L, Cui X, Zhang J, Wang K, Shen M, Zeng S, Dayeh S A, Feng L and Xiang B 2014 *Sci. Rep.* **4** 5649
[33] Li H, Contryman A W, Qian X F, Ardakani S M, Gong Y J, Wang X L, Weisse J M, Lee C H, Zhao J H, Ajayan P M, Li J, Manoharan H C and Zheng X L 2015 *Nat. Commun.* **6** 7381
[34] Lloyd D, Liu X, Christopher J W, Cantley L, Wadehra A, Kim B L, Goldberg B B, Swan A K and Bunch J S 2016 *Nano Lett.* **16** 5836
[35] Robinson B J, Giusca C E, Gonzalez Y T, Kay N D, Kazakova O and Kolosov O V 2015 *2D Mater.* **2** 015005
[36] Kwon S, Kwon M H, Song J, Kim E, Kim Y, Kim B R, Hyun J K, Lee S W and Kim D W. 2019 *Sci. Rep.* **9** 14434
[37] Li F, Qi J, Xu M, Xiao J, Xu Y, Zhang X, Liu S and Zhang Y 2017 *Small* **13** 1603103
[38] Markeev P A, Najafidehaghani E, Gan Z, Sotthewes K, George A, Turchanin A and Jong M P 2021 *J. Phys. Chem. C* **125** 13551